Conformability of a Thin Elastic Membrane Laminated on a Soft Substrate With Slightly Wavy Surface

Liu Wang
Center for Mechanics of Solids,
Structures and Materials,
Department of Aerospace Engineering
and Engineering Mechanics,
The University of Texas at Austin,
Austin, TX 78712

Nanshu Lu[1]
Center for Mechanics of Solids,
Structures and Materials,
Department of Aerospace Engineering
and Engineering Mechanics,
The University of Texas at Austin,
Austin, TX 78712;
Department of Biomedical Engineering,
The University of Texas at Austin,
Austin, TX 78712;
Texas Materials Institute,
The University of Texas at Austin,
Austin, TX 78712
e-mail: nanshulu@utexas.edu

When laminating a thin elastic membrane on a substrate with surface roughness, three scenarios can happen: fully conformed (FC), i.e., the membrane completely follows the surface morphology of the substrate without any interfacial gap, nonconformed (NC), i.e., the membrane remains flat if gravity is not concerned, and partially conformed (PC). Good conformability can enhance effective membrane-to-substrate adhesion strength and can facilitate signal/heat/mass transfer across the interface, which are of great importance to soft electronics laminated on rough bio-tissues. To reveal governing parameters in this problem and to predict conformability, energy minimization is implemented after successfully finding the substrate elastic energy under partially conformable contact. Four dimensionless governing parameters involving the substrate roughness, membrane thickness, membrane and substrate elastic moduli, and membrane-to-substrate intrinsic work of adhesion have been identified to analytically predict the conformability status and the area of contact. The analytical prediction has found excellent agreement with experimental observations. In summary, an experimentally validated quantitative guideline for the conformability of elastic membrane on soft corrugated substrate has been established in the four-parameter design space. [DOI: 10.1115/1.4032466]

Keywords: thin film, soft substrate, corrugated surface, conformability, adhesion

1 Introduction

Even a highly polished surface has surface roughness. For example, the root-mean-square (rms) roughness of a high-end polished silicon wafer is 0.3 nm [1], and the rms roughness of human skin ranges from 0.03 μm to 45 μm [2]. When a thin membrane is brought into contact with a rough substrate, we expect three contact modes: (1) FC mode as illustrated in Fig. 1(a), i.e., the membrane completely covers the surface of the substrate without any interfacial gap; (2) PC mode as depicted in Fig. 1(b), i.e., some part of the membrane forms intimate contact with the substrate surface while other part of the membrane is suspended; (3) NC mode as shown in Fig. 1(c), i.e., the membrane remains flat if gravity is neglected.

Conformability governs the effective adhesion strength between a thin film and a rough surface. Higher effective adhesion strength can be achieved by improving film-to-substrate conformability. For example, monolayer graphene to silicon adhesion strength is measured to be higher than few layer graphene (FLG) [3], which is attributed to better conformability between monolayer graphene and the silicon substrate [4]. As another example, the feet of geckos and beetles are covered by thin fibers ending with leaflike plates which can be easily bent to well conform to rough contacting surface, which considerably enhances the adhesion strength [5,6]. Moreover, conformability-based metrology has been applied to estimate the adhesion strength between FLG and a precorrugated polydimethylsiloxane [7].

In addition to adhesion strength, conformability of thin membranes on rough surfaces also plays a significant role in the functionality of bio-integrated electronics [8], which have sprung up in recent years due to unlimited potentials in disease monitoring, diagnosis, treatment, as well as human–machine interfaces. Intimate contact between device sheet and bio-tissue is required for superior signal-to-noise ratio in both implantable [9,10] and epidermal [11–14] electrophysiological sensors, hydration sensors [15], and temperature detectors [16]. As another example, wearable heaters for thermoregulation and thermal treatment [17,18] require uniform and efficient heat transfer at the heater–tissue interface, which fully relies on intimate heater–tissue contact. Moreover, effective device–tissue interface mass exchange for sweat monitoring [19,20] and on-demand drug delivery [21] would also benefit from conformable device–tissue contact.
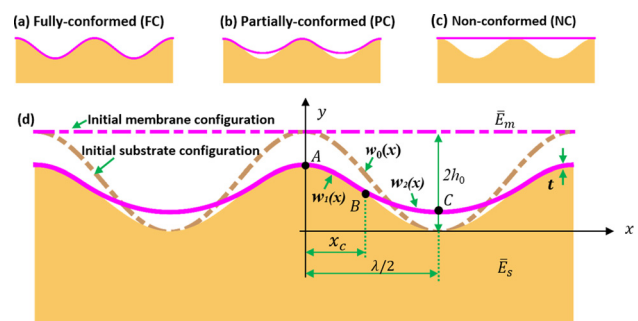

Fig. 1 Three possible conformability status when a thin elastic membrane is laminated on a sinusoidally corrugated substrate: (a) FC, (b) PC, and (c) NC. (d) Schematic of PC scenario with geometric parameters and characteristic points labeled: the initial amplitude and wavelength of the substrate are $2h_0$ and λ, respectively; after membrane lamination, the substrate surface within the contact zone deforms to a new sinusoidal shape with amplitude $2h_1$ (not labeled in the figure) and unchanged wavelength; x_c is the horizontal projection of the contact zone; and point B denotes the delaminating point.

Therefore, a comprehensive mechanistic understanding on the conformability of thin device sheets on soft bio-tissues can offer important insights into the design of the mechanical properties of the bio-integrated devices.

The conformability of a thin membrane on a rigid substrate with corrugated surface has been studied. For example, in the case of graphene sheets laminated on silicon substrate, Gao and Huang developed a theoretical model based on van der Waals interaction to reveal how the graphene thickness and the surface roughness of silicon affect the conformability [4]. Wagner and Vella implemented the method of variation of total energy to show that the substrate profile plays a crucial role in determining the transition from partial to full conformability [22]. Furthermore, using energy minimization method, Qiao et al. established a complete theory to predict the FC, PC, and NC modes of a thin membrane on a rigid and corrugated substrate [23]. In fact, conformal contact and effective adhesion strength between a thin elastic plate and a rigid and randomly rough (e.g., self-affine fractal) substrate have been studied by Carbone et al. using contact mechanics [24].

When the substrate is a soft solid with surface roughness, it can deform due to film–substrate interaction and would also try to conform to the film. Conformability of thin membrane on rough, deformable substrate still remains veiled so far due to the unclear interaction between the membrane and the soft substrate, especially for PC cases. As a result, the elastic energy stored in the deformed substrate is difficult to obtain unless the corrugated substrate surface deforms from one sinusoidal shape to another sinusoidal shape with the same wavelength but different amplitudes, which requires FC contact between the membrane and substrate. In this case, analytical solutions of the surface traction and displacement of the substrate are available [25,26]. Based on those analytical solutions, substrate elastic energy can be computed as the work done to the substrate and hence can be used to predict whether epidermal electronics can fully conform to rough skin surfaces using the energy minimization method [27,28].

However, when the film only partially conforms to the substrate, film–substrate interaction and substrate surface displacement are not readily available. We would like to solve for the partially conformable mode because it is a very common scenario and we will be able to predict the actual area of contact. In the case of bio-integrated electronics, bio-tissues like the skin or the brain generally have a small surface roughness compared with the wavelength of the corrugation [2,10,29]; therefore, in this paper, we limit ourselves to the following essential assumptions:

(i) The soft substrate has a slightly wavy surface, i.e., the amplitude-to-wavelength ratio is smaller than 0.2.
(ii) Within the contact zone, the substrate surface deforms from one sinusoidal shape to another with the same wavelength but a different amplitude.
(iii) Shear stress on the membrane–substrate interface is neglected [25].

Assumption (ii) originates from the FC scenario [27,28] and is an approximation for slightly wavy surfaces. In Sec. 4, we will double check if assumption (ii) can lead to the existing FC results. Since there is no traction applied on the noncontacting substrate surface, no work is done to the substrate in this area even if there is displacement. Therefore, there is no need to solve for the displacement of the substrate surface in the noncontacting zone (although we will still provide it in Sec. 4). Since the elastic energy stored in the substrate equals to the work done to the substrate, as long as we can determine both the displacement and the traction on the substrate surface within the contact zone, we can use energy minimization method to analytically search for the equilibrium configuration and hence predict the conformability modes as a result of substrate surface roughness, film thickness, film and substrate moduli, as well as film–substrate intrinsic work of adhesion. The theoretical model will be discussed in Sec. 2, and two experimental validations (Ecoflex on skin replica and polyimide (PI) on brain tissue) are performed in Sec. 3. Further

discussions and concluding remarks are presented in Secs. 4 and 5, respectively.

2 Theoretical Model

A 2D schematic for the PC configuration is given in Fig. 1(d). For simplicity, the membrane is modeled as a uniform linear elastic membrane with plane strain modulus $\bar{E}_m$ and thickness t. The soft substrate is assumed to be a precorrugated linear elastic half space with plane strain modulus $\bar{E}_s$. Within the Cartesian coordinate system xy as defined in Fig. 1(d), the surface profile of the undeformed substrate is simply characterized by a sinusoidal equation

$$w_0(x) = h_0\left(1 + \cos\frac{2\pi x}{\lambda}\right) \tag{1}$$

where h_0 and λ denote the semi-amplitude and wavelength of the undeformed substrate surface, respectively.

When an elastic membrane is laminated on the soft substrate and starts to conform to the substrate due to interface adhesion, a contact zone with horizontal projection denoted as x_c is labeled in Fig. 1(d). Therefore, $x_c = \lambda/2$ represents FC scenario (Fig. 1(a)), $0 < x_c < \lambda/2$ PC scenario (Fig. 1(b)), and $x_c = 0$ NC scenario (Fig. 1(c)). Due to the membrane–substrate interaction, the soft substrate deforms. Here, we simply postulate that the surface profile of the substrate within the contact zone deforms from the initial sinusoidal shape to a new sinusoidal shape with the same wavelength but a different amplitude, which can be captured by

$$w_1(x) = h_1\left(1 + \cos\frac{2\pi x}{\lambda}\right), \quad 0 \le x \le x_c \tag{2}$$

where h_1 denotes the deformed semi-amplitude while the wavelength λ remains the same as the initial profile. This assumption holds all the way till $x_c = \lambda/2$, which means in the FC mode, the overall substrate surface deforms from one sinusoidal profile to another with the same wavelength but different amplitudes.

The profile of a PC membrane, $w_2(x)$, as depicted in Fig. 1(d), is sectional: from A to B, i.e., when $0 \le x \le x_c$, the membrane fully conforms to the substrate and thus $w_2(x) = w_1(x)$; from B to C, i.e., when $x_c \le x \le \lambda/2$, the membrane is suspended, and $w_2(x)$ is taking a modified hyperbolic shape which will decay to a parabolic shape when normal strain in the membrane is small, i.e., a pure bending condition is assumed [22,23]. Therefore, $w_2(x)$ can be expressed as

$$w_2(x) = \begin{cases} h_1\left(1 + \cos\frac{2\pi x}{\lambda}\right), & 0 \le x \le x_c \\ a\left(x - \frac{\lambda}{2}\right)^2 + b, & x_c \le x \le \lambda/2 \end{cases} \tag{3}$$

where a and b are the two coefficients to be determined by the continuity condition. Applying the continuity condition at point B where both the profile and the slope of the membrane should be continuous, i.e., $w_2(x_c) = w_1(x_c)$ and $w_2'(x_c) = w_1'(x_c)$, we can solve the coefficients a and b to obtain the profile of the membrane from B to C as

$$w_2(x) = h_1\left[\frac{\pi}{\lambda\left(\frac{\lambda}{2} - x_c\right)}\sin\left(\frac{2\pi x_c}{\lambda}\right)\left[\left(x - \frac{\lambda}{2}\right)^2 - \left(x_c - \frac{\lambda}{2}\right)^2\right]\right.$$
$$\left. + 1 + \cos\left(\frac{2\pi x_c}{\lambda}\right)\right], \quad x_c \le x \le \lambda/2 \tag{4}$$

To solve for x_c and h_1 in Eq. (4), energy minimization method is adopted. The total energy of the system U_{total} consists of the following four energies:

$$U_{\text{total}} = U_{\text{bending}} + U_{\text{membrane}} + U_{\text{adhesion}} + U_{\text{substrate}} \quad (5)$$

where U_{bending} is the bending energy of the membrane, U_{membrane} is the membrane energy associated with tensile strain in the membrane, U_{adhesion} is the interface adhesion energy between the membrane and the substrate, and $U_{\text{substrate}}$ is the elastic energy stored in the substrate, will have to be obtained through contact mechanics analysis. None of the four energies can be neglected in our analysis. Both bending and membrane energies are making significant contributions according to our recent paper of elastic membranes laminated on rigid corrugated substrate [23]. Adhesion energy helps reduce the total energy of the system and is the only negative component out of the four. Nonzero elastic energy stored in the substrate indicates that the substrate is a deformable object, which is the key to this paper.

The bending energy of the membrane (per unit arc length) is given by

$$U_{\text{bending}} = \frac{2}{\lambda}\left[\frac{1}{2}\int_A^B \bar{E}_m I \kappa_1^2 ds + \frac{1}{2}\int_B^C \bar{E}_m I \kappa_2^2 ds\right] \quad (6)$$

where $\bar{E}_m I = \bar{E}_m t^3/12$ is the plane strain bending stiffness of the membrane, κ is its curvature, and ds is the infinitesimal arc length. We use subscript 1 to represent the contact zone, i.e., from A to B, and subscript 2 to denote the noncontacting zone, i.e., from B to C, as labeled in Fig. 1(d). The membrane energy per unit arc length can be written as

$$U_{\text{membrane}} = \frac{2}{\lambda}\left[\frac{1}{2}\int_A^B \bar{E}_m t \epsilon_1^2 ds + \frac{1}{2}\int_B^C \bar{E}_m t \epsilon_2^2 ds\right] \quad (7)$$

where $\epsilon_1(x) = \sqrt{1 + w_1'^2} - 1$ and $\epsilon_2(x) = \sqrt{1 + w_2'^2} - 1$ are the tensile strains in the adhered and noncontacting zones of the membrane, respectively. Adhesion between the membrane and the substrate actually reduces system energy so it should be negative. Given the membrane–substrate interface work of adhesion γ, adhesion energy per arc length becomes

$$U_{\text{adhesion}} = -\frac{2}{\lambda}\int_A^B \gamma ds \quad (8)$$

For analytical computation of these energies, simplification and nondimensionalization are implemented. Since a slightly wavy surface is considered, the deflection of the membrane is assumed to be small. Therefore, approximations can be applied to simplify the computation of bending energy, which are $\kappa_i \approx w_i''$ ($i = 1, 2$) and $ds \approx dx$. Hence, the bending energy can be written as

$$U_{\text{bending}} = \frac{2}{\lambda}\left[\frac{1}{2}\int_0^{x_c} \bar{E}_m I (w_1'')^2 dx + \frac{1}{2}\int_{x_c}^{\frac{\lambda}{2}} \bar{E}_m I (w_2'')^2 dx\right]$$
$$= \frac{4\pi^2 h_1^2 \bar{E}_m I}{\lambda^4} D(\hat{x}_c) \quad (9)$$

where

$$D(\hat{x}_c) = \frac{2}{1 - \hat{x}_c}\sin^2(\pi\hat{x}_c) + \pi^2\hat{x}_c + \frac{\pi}{2}\sin(2\pi\hat{x}_c) \quad (10)$$

and $\hat{x}_c = 2x_c/\lambda$ is the dimensionless parameter that describes the degree of conformability: $\hat{x}_c = 0$ represents NC, $0 < \hat{x}_c < 1$ means PC, and $\hat{x}_c = 1$ denotes FC. If we define three more dimensionless parameters $\beta = 2\pi h_0/\lambda$, $\eta = t/\lambda$, and $\xi = h_1/h_0$ and

substitute $\bar{E}_m I = \bar{E}_m t^3/12$, we can further express bending energy per unit arc length as

$$U_{\text{bending}} = \frac{4\pi^2 h_1^2 \bar{E}_m I}{\lambda^4} D(\hat{x}_c) = \bar{E}_m \lambda \frac{\beta^2 \xi^2}{12} \eta^3 D(\hat{x}_c) \quad (11)$$

As for the computation of membrane energy and adhesion energy, arc length is taken as $ds \approx \sqrt{1 + (w_i')^2}dx \approx [1 + 1/2(w_i')^2]dx$ (otherwise, strain $\epsilon_i(x) = (ds - dx)/dx$ is zero if $ds \approx dx$). Hence, membrane energy becomes

$$U_{\text{membrane}} = \frac{1}{\lambda}\left[\int_0^{x_c} \bar{E}_m t\left(\frac{1}{2}(w_2')^2\right)^2\left(1 + \frac{1}{2}(w_2')^2\right)dx\right.$$
$$\left. + \int_{x_c}^{\frac{\lambda}{2}} \bar{E}_m t\left(\frac{1}{2}(w_2')^2\right)^2\left(1 + \frac{1}{2}(w_2')^2\right)dx\right]$$
$$= \bar{E}_m \lambda \ \eta \ (\beta\xi)^4 K(\hat{x}_c, \xi\beta) \quad (12)$$

where

$$K(\hat{x}_c, \xi\beta)$$
$$= \frac{\beta^2}{107520\pi}\Big(96\pi(-1 + \hat{x}_c)(-28 - 5\beta^2 + 5\beta^2 \cos(2\pi\hat{x}_c))$$
$$\times \sin(\pi\hat{x}_c)^4 + 35\big(144\pi\hat{x}_c + 60\beta^2\pi\hat{x}_c - 3(32 + 15\beta^2)$$
$$\times \sin(2\pi\hat{x}_c) + 3(4 + 3\beta^2)\sin(4\pi\hat{x}_c) - \beta^2 \sin(6\pi\hat{x}_c)\big)\Big) \quad (13)$$

And, adhesion energy can be calculated as

$$U_{\text{adhesion}} \approx -\frac{2\gamma}{\lambda}\int_0^{x_c}\left(1 + \frac{1}{2}(w_2')^2\right) dx = -\gamma E(\hat{x}_c, \ \xi\beta) \quad (14)$$

where

$$E(\hat{x}_c, \ \xi\beta) = \hat{x}_c\left(1 + \frac{(\xi\beta)^2}{4\pi}\right) - \frac{(\xi\beta)^2}{8\pi} \ \sin(2\pi\hat{x}_c) \quad (15)$$

The calculation of the elastic energy stored in the substrate $U_{\text{substrate}}$ is not as straightforward because the traction between membrane and substrate is not readily known. According to assumption (ii), displacement of the substrate surface within the contact zone can be calculated as

$$u(x) = w_1(x) - w_0(x) = (h_1 - h_0)\left(1 + \cos\frac{2\pi x}{\lambda}\right), \quad 0 \le x \le x_c \quad (16)$$

For the surface traction $P(x)$ over the contact zone as labeled in Fig. 2, if we just focus on the elastic substrate with a slightly wavy surface, Johnson [30] has a conclusion that is directly applicable to our situation. He claimed that $P(x)$ can be comprehended by the superposition of a compressive pressure $P_1(x)$ and a tensile pressure $P_2(x)$, which follows as:

$$P(x) = P_1(x) + P_2(x), \quad 0 \le x \le x_c \quad (17)$$

Here, $P_1(x)$ is the so-called "bearing pressure" which induces a sinusoidal surface displacement $u(x)$ on a soft substrate with either flat or a slightly wavy surface. The contact of two slightly wavy half-planes in the absence of adhesion (Fig. 3(a)) was first
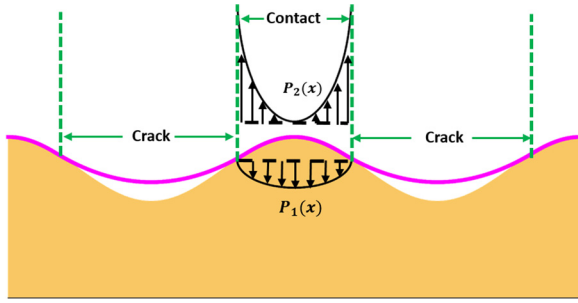
Fig. 2 Schematic of traction over the contact area in the presence of adhesion by superposition $P(x) = P_1(x) + P_2(x)$, where $P_1(x)$ is given by Eq. (18) and $P_2(x)$ is given by Eq. (19)
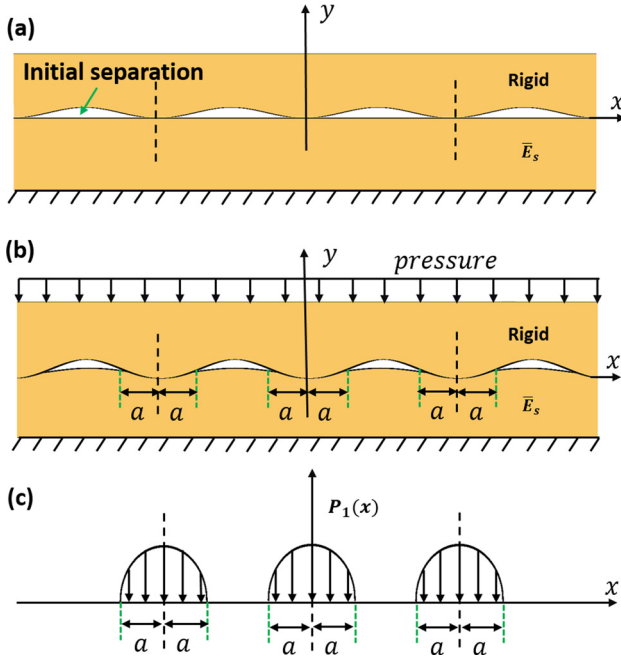

Fig. 3 (a) Schematic of a rigid, slightly wavy surface with periodicity λ touching a flat elastic surface before any deformation. (b) When subjected to uniform external pressure periodic, sinusoidal displacement is induced in the contact zone $(-x_c < x < x_c)$. (c) Distribution of the bearing pressure, $P_1(x)$ as given by Eq. (18), within the contact zone.

analyzed by Westergaard [31]. When a rigid body with a slightly wavy surface is compressed against an infinitely large elastic substrate with flat surface as depicted in Fig. 3(b), contact occurs over width $2a$ near the crests of the waves. For small amplitude corrugation, following Westergaard's solution [31], the bearing pressure distribution over contact zone, i.e., $0 \leq x \leq x_c$ in our case, can be expressed as:

$$P_1(x) = -2\pi \bar{E}_s \frac{h_0 - h_1}{\lambda} \cos \frac{\pi x}{\lambda}$$
$$\times \sqrt{\left(\sin \frac{\pi x_c}{\lambda}\right)^2 - \left(\sin \frac{\pi x}{\lambda}\right)^2}, \quad 0 \leq x \leq x_c \quad (18)$$

where the forefront negative sign suggests that $P_1(x)$ is a compressive pressure. The profile of $P_1(x)$ is depicted in Fig. 3(c).

When adhesion is taken into account, it will facilitate the two contacting surfaces to be attracted to each other, hence we expect
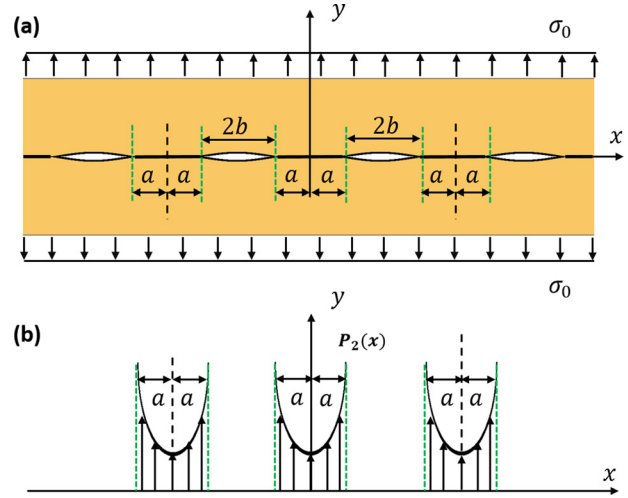
Fig. 4 (a) A row of collinear cracks in an infinite elastic sheet with crack length $2a$ and interval $2b$, subjected to remote tensile stress σ_0. (b) Stress distribution over the ligament represents the adhesion stress $P_2(x)$ as given by Eq. (19).

$P_2(x)$ to be a tensile (or positive) pressure. Johnson [30] suggested that $P_2(x)$ can be comprehended as the stress distributed across the ligament $(-a < x < a)$ on a plane of collinear, periodic cracks each of length $2b$ under remote tensile loading σ_0 (Fig. 4(a)). In this drawing, the ligament represents the contact zone and the crack represents the noncontact zone as shown in Fig. 2. The problem of collinear cracks in an infinite elastic sheet was analyzed by Koiter [32], who offered the stress distribution over the contact zone, i.e., $0 \leq x \leq x_c$ in our case, as

$$P_2(x) = \sigma_0 \cos \frac{\pi x}{\lambda} \left[\sqrt{\left(\cos \frac{\pi x}{\lambda}\right)^2 - \left(\cos \frac{\pi x_c}{\lambda}\right)^2} \right]^{-1}, \quad 0 \leq x \leq x_c$$
$$(19)$$

whose profile is drawn in Fig. 4(b). Here, σ_0 can be determined by letting the averaged overall traction $\bar{P}$ (Fig. 2) go zero as the membrane spontaneously conforms to the substrate without any external load [33]

$$\bar{P} = \int_{-x_c}^{x_c} P(x)dx = \int_{-x_c}^{x_c} [P_1(x) + P_2(x)]dx = 0 \quad (20)$$

Solving Eq. (20) yields

$$\sigma_0 = \pi \bar{E}_s \frac{h_0 - h_1}{\lambda} \left(\sin \frac{\pi x_c}{\lambda} \right)^2 \quad (21)$$

which means that the total traction within contact zone in the presence of adhesion as given by Eq. (17) is now fully solved. Hence, elastic energy stored in the substrate $U_{\text{substrate}}$ per unit arc length can be obtained as the product of traction and displacement

$$U_{\text{substrate}} = \frac{2}{\lambda} \int_0^{x_c} \frac{1}{2} u(x)P(x)dx = \frac{1}{\lambda} \int_0^{x_c} u(x)[P_1(x) + P_2(x)]dx$$
$$= \frac{(h_0 - h_1)^2 \bar{E}_s \pi}{\lambda} [F_1(\hat{x}_c) - F_2(\hat{x}_c)]$$
$$= \frac{\bar{E}_s \lambda \beta^2 (1 - \xi)^2}{4\pi} [F_1(\hat{x}_c) - F_2(\hat{x}_c)] \quad (22)$$

where $F_1(\hat{x}_c)$ and $F_2(\hat{x}_c)$ are the two dimensionless functions

$$F_1(\hat{x}_c) = \frac{1}{\lambda} \int_0^{x_c} 2\left(1 + \cos\frac{2\pi x}{\lambda}\right)\cos\frac{\pi x}{\lambda}$$
$$\times \sqrt{\left(\sin\frac{\pi x_c}{\lambda}\right)^2 - \left(\sin\frac{\pi x}{\lambda}\right)^2} \, dx$$
$$F_2(\hat{x}_c) = \frac{1}{\lambda} \int_0^{x_c} \left(1 + \cos\frac{2\pi x}{\lambda}\right)\left(\sin\frac{\pi x_c}{\lambda}\right)^2$$
$$\times \cos\frac{\pi x}{\lambda}\left[\sqrt{\left(\cos\frac{\pi x}{\lambda}\right)^2 - \left(\cos\frac{\pi x_c}{\lambda}\right)^2}\right]^{-1} dx \quad (23)$$

Taylor expansion of $P_1(x)$ and $P_2(x)$ up to $O(x^6)$ is applied to numerically solve $U_{\text{substrate}}$.

Hence, the total energy of the system can be explicitly expresses as

$$U_{\text{total}} = \bar{E}_m\lambda\frac{\beta^2\xi^2}{12} \eta^3 D(\hat{x}_c) + \bar{E}_m\lambda \, \eta \, (\beta\xi)^4 K(\hat{x}_c, \xi\beta)$$
$$- \gamma E(\hat{x}_c, \ \xi\beta) + \frac{\bar{E}_s\lambda\beta^2(1-\xi)^2}{4\pi}[F_1(\hat{x}_c) - F_2(\hat{x}_c)] \quad (24)$$

Through dimensional analysis, we want to introduce two additional dimensionless parameters $\alpha = \bar{E}_m/\bar{E}_s$ and $\mu = \gamma/(\bar{E}_s\lambda)$, which are membrane-to-substrate modulus ratio and normalized interface intrinsic work of adhesion. Finally, the normalized total energy becomes

$$\hat{U} = \frac{U_{\text{total}}}{\bar{E}_s\lambda\beta^2}$$
$$= \alpha\frac{\xi^2}{12} \eta^3 D(\hat{x}_c) + \alpha \, \eta \, \xi^4\beta^2 K(\hat{x}_c, \xi\beta) - \frac{\mu}{\beta^2}E(\hat{x}_c, \ \xi\beta)$$
$$+ \frac{(1-\xi)^2}{4\pi}[F_1(\hat{x}_c) - F_2(\hat{x}_c)] \quad (25)$$

which is a function of four dimensionless input parameters: $\beta = 2\pi h_0/\lambda, \eta = t/\lambda, \ \alpha = \bar{E}_m/\bar{E}_s$, and $\mu = \gamma/(\bar{E}_s\lambda)$, which are physically interpreted as normalized roughness of the corrugated substrate (β), normalized membrane thickness (η), membrane-to-substrate modulus ratio (α), and normalized membrane–substrate intrinsic work of adhesion (μ), respectively. In addition, there are two unknown dimensionless parameters: $\hat{x}_c = 2x_c/\lambda$ and $\xi = h_1/h_0$, which once solved can yield the contact zone and the amplitude of the deformed substrate. By fixing $\beta, \alpha, \ \mu$, and η, minimization of Eq. (25) with respect to $\hat{x}_c$ and ξ within the domain confined by $0 \leq \hat{x}_c \leq 1$ and $0 \leq \xi \leq 1$ will give us the equilibrium solution, which can be visualized as the global minimum of the 3D plot of the normalized total energy landscape as a function of $\hat{x}_c$ and ξ.

3 Experimental Validation

With the total energy obtained in Eq. (25), we are now ready to implement the energy minimization method to predict conformability conditions of thin membranes laminated on soft, corrugated substrates. Two experiments in the literature are adopted to validate our model.

3.1 Ecoflex Membrane on Skinlike Substrate. Epidermal electronics can be exploited for many clinical and research purposes. Due to the ultimate thinness and softness of epidermal sensors, laminating them on microscopically rough skin surface leads to fully conformal contact, which can maximize the signal-to-noise ratio while minimize motion artifacts, as evidenced in Ref. [34]. To optimize the design of epidermal electronics for

human–machine interface, Jeong et al. [13] tested the conformability of elastomer membranes (Ecoflex, Smooth-On, USA) of various thicknesses on an Ecoflex replica of the surface of human skin. Membrane–substrate conformability is clearly revealed by the cross-sectional scanning electron microscopy images (Fig. 2(a) in Ref. [13]): 5 μm thick membrane can achieve full conformability to the substrate, 36 μm thick membrane only PC to the substrate, whereas membranes with thickness of 100 μm and 500 μm remained NC at all. Basic parameters that can be extracted from the experiments are: substrate roughness $h_0 = 50 \, \mu\text{m}$, $\lambda = 250 \, \mu\text{m}$, plane strain moduli of membrane, and substrate $\bar{E}_s = \bar{E}_m = 92$ kPa [13]. Since the conformability experiments were carried by placing Ecoflex membrane on Ecoflex-based skin replica, we assume the interface intrinsic work of adhesion to be $\gamma = 50 \, \text{mJ/m}^2$ according to our recent experimental measurements on the work of adhesion between different types of elastomers [35]. Based on those given parameters, the four dimensionless parameters are computed as follows: $\beta = 1.2, \alpha = 1, \mu = 0.003$, and $\eta = 0.02, 0.144, 0.4$, and 2, which corresponds to the four different experimental thicknesses of the membrane $t = 5 \, \mu\text{m}, 36 \, \mu\text{m}, 100 \, \mu\text{m}, 500 \, \mu\text{m}$, respectively. Normalized total energy given by Eq. (25) of each η is calculated, and the energy landscape $\hat{U}$ versus $\hat{x}_c$ and ξ is plotted in Figs. 5(a)–5(d). When $\eta = 0.02$ (Fig. 5(a)), the global minimum falls at $\hat{x}_c = 1$ and $\xi = 0.88$, as highlighted by the red dot in the figure and the inset. $\hat{x}_c = 1$ indicates full conformability and $\xi = 0.88$ suggests that the substrate is flattened to a new amplitude of $h_1 = 0.88h_0$. When $\eta = 0.144$ (Fig. 5(b)), the minimal energy locates at $\hat{x}_c = 0.09$, $\xi = 0.65$, indicating a PC scenario where contact zone only covers about 9% of the wavelength. As for $\eta = 0.4$ (Fig. 5(c)) and $\eta = 2$ (Fig. 5(d)), the minimal energy points are both at $\hat{x}_c = 0$, $\xi = 1$, suggesting that the membrane is nonconformal to the substrate and the substrate is not deformed at all. Therefore, our predictions of conformability for four different membrane thicknesses are in excellent agreement with the experimental findings.

By fixing the substrate morphology $\beta = 1.2$ (i.e., $h_0 = 50 \, \mu\text{m}$ and $\lambda = 250 \, \mu\text{m}$), Fig. 6 predicts the conformability as a function of the other three parameters α, μ, and η. By numerically solving the minimization problem above, a 3D plot in Fig. 6(a) shows two critical surfaces dividing FC/PC and PC/NC. It is obvious that the FC condition can be achieved at small η, i.e., thinner membrane, small α, i.e., softer membrane compared to the substrate, and large μ, i.e., strong membrane–substrate intrinsic work of adhesion. On the contrary, NC condition most likely occurs at large α, large η, and small μ.

To better illustrate the effect of individual variables, we choose to fix three variables and only change one at a time. For example, in Fig. 6(b), $\hat{x}_c$ is plotted as a function of η in the top axis and t in the bottom axis with $\beta = 1.2$, $\alpha = 1$, and $\mu = 0.003$ fixed. It is evident that as the film thickness grows from 0, the conformability goes from FC to PC and finally NC. While the transition from PC to NC is smooth, the transition from FC to PC is abrupt, which suggests a significant drop (>77%) of contact area from FC to PC. Similar jump has been observed for FLG conforming to silicon substrate [36] and elastic membrane laminated on rigid, corrugated substrate [23]. More analysis on how different substrate morphologies affect snap-through transition can be found in Ref. [22]. Quantitatively, full conformability requires $\eta < 0.03$, i.e., $t < 7.5 \, \mu\text{m}$. When $\eta > 0.28$, i.e., $t > 70 \, \mu\text{m}$, there is no conformability at all. When $0.03 < \eta < 0.28$, i.e., when $7.5 \, \mu\text{m} < t < 70 \, \mu\text{m}$, the contact area of the PC scenario can be determined. The three black dots indicate the three different membrane thicknesses tested in the experiments by Jeong et al. [13], which are fully consistent with our prediction.

Since the original epidermal electronics was fabricated on 30 μm thick Ecoflex [12], the conformability of a 30 μm thick membrane on an Ecoflex skin replica substrate has been predicted. In order to show the effect of adhesion energy and membrane modulus over wide range, $\hat{x}_c$ versus μ (or γ) and $\hat{x}_c$ versus α
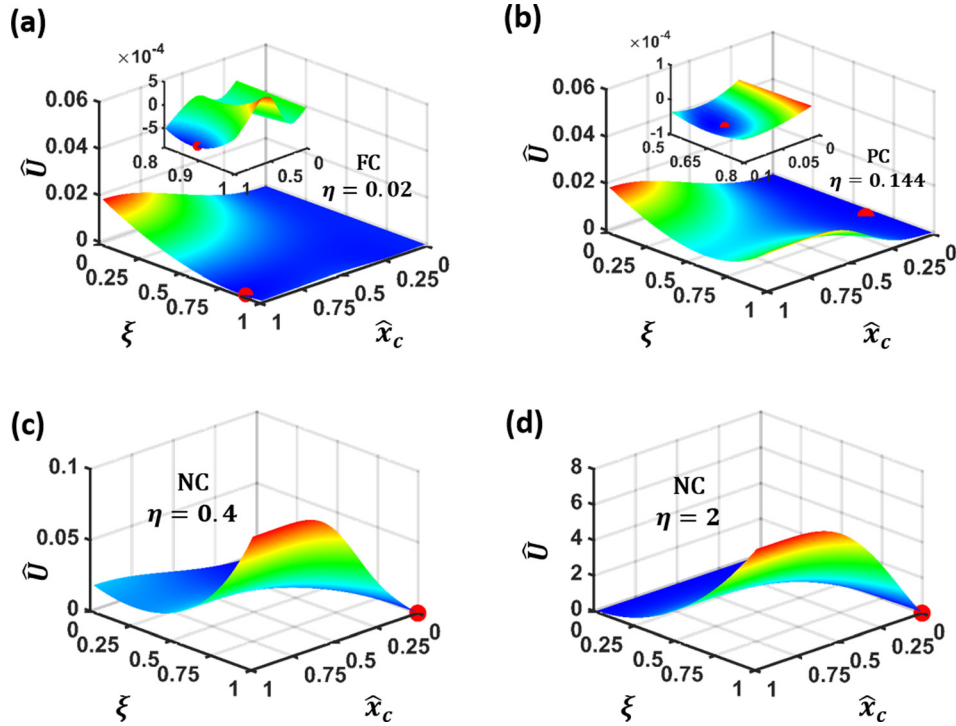
Fig. 5 Normalized total energy landscape of Ecoflex membrane of four different thicknesses (four different η's) laminating on Ecoflex skin replica, where $\alpha = 1$, $\beta = 1.2$, and $\mu = 0.003$. Global minima are labeled by red dots. (a) When $\eta = 0.02$, $\hat{x}_c = 1$, and $\xi = 0.88$, it indicates FC. (b) When $\eta = 0.0144$, $\hat{x}_c = 0.09$, $\xi = 0.65$, it predicts PC. (c) When $\eta = 0.4$ and (d) when $\eta = 2$, $\hat{x}_c = 0$, and $\xi = 1$, it suggests NC.
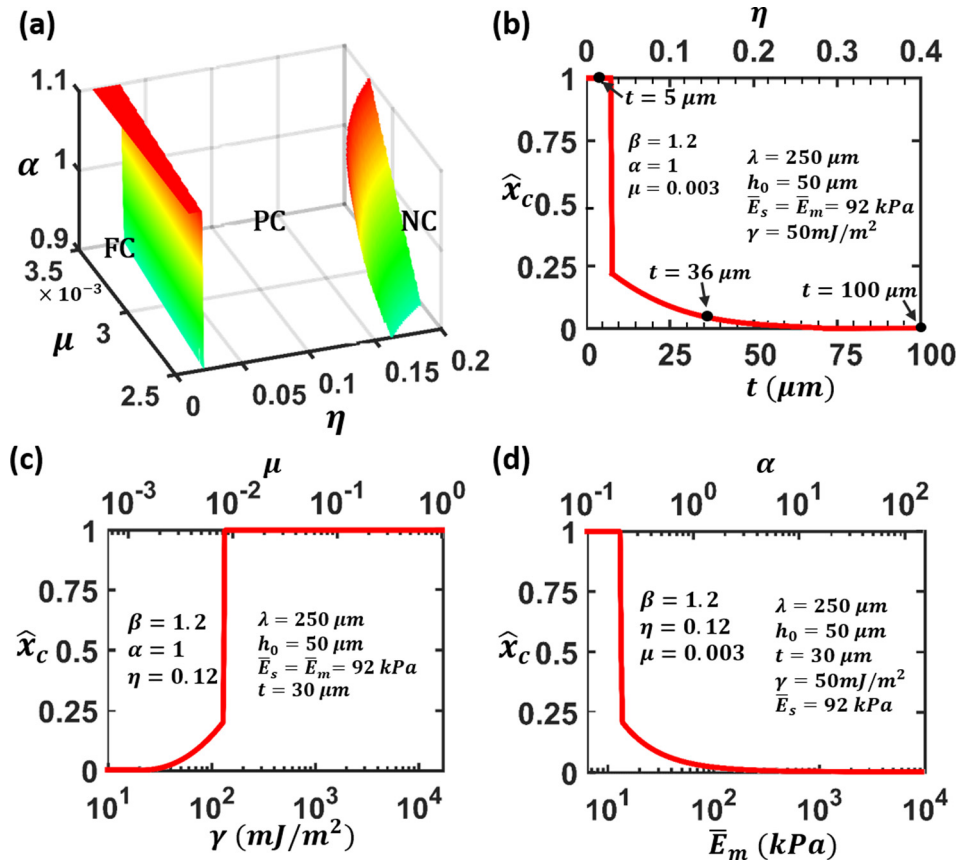

Fig. 6 (a) Surfaces dividing FC/PC and PC/NC when $\beta = 1.2$ (i.e., $h_0 = 50\,\mu m$ and $\lambda = 250\,\mu m$) is fixed. (b) Contact area $\hat{x}_c$ versus η on the top or t in the bottom when $\beta = 1.2$, $\alpha = 1$, and $\mu = 0.003$. (c) Contact area $\hat{x}_c$ versus μ when $\beta = 1.2$, $\alpha = 1$, and $\eta = 0.12$. (d) Contact area $\hat{x}_c$ versus α when $\beta = 1.2$, $\mu = 0.003$, and $\eta = 0.12$.
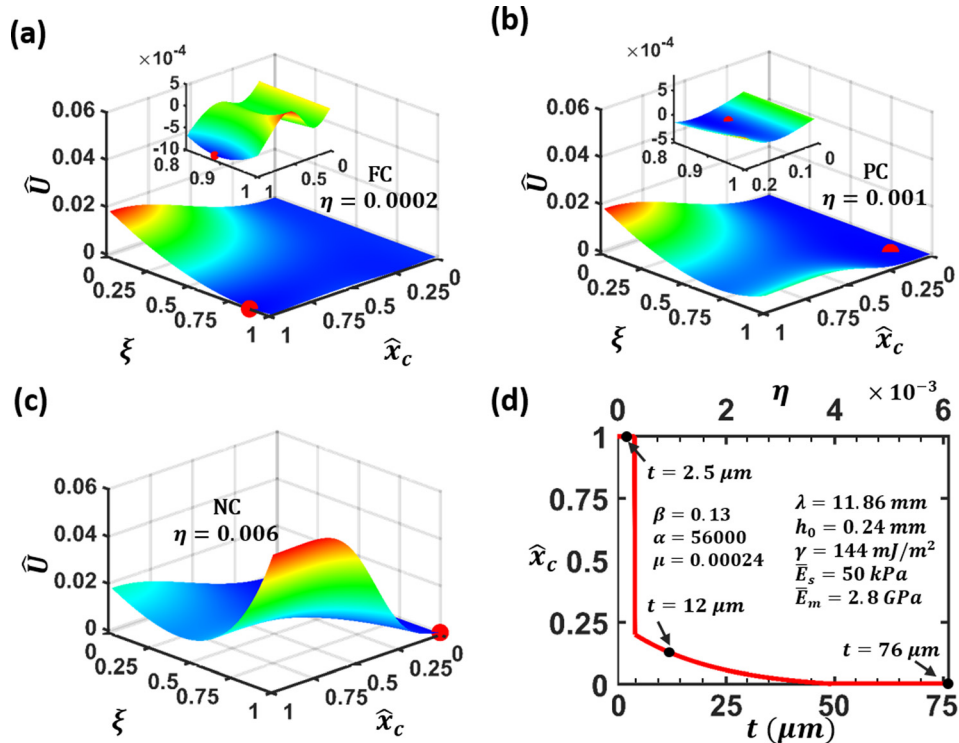
Fig. 7 (*a*)–(*c*) Normalized total energy landscape of PI supported electrodes of three different thicknesses (i.e., three different η's) laminated on feline cortex when $\beta = 0.13, \alpha = 56,000$, and $\mu = 2.4 \times 10^{-4}$. (*a*) When $\eta = 0.0002$, $\hat{x}_c = 1$, and $\xi = 0.9$, it indicates FC. (*b*) When $\eta = 0.001$, $\hat{x}_c = 0.12$, and $\xi = 0.86$, it predicts PC. (*c*) When $\eta = 0.006$, $\hat{x}_c = 0$, and $\xi = 1$, it suggests NC. (*d*) Contact area $\hat{x}_c$ versus η on the top or t in the bottom when $\beta = 0.06$, $\alpha = 56,000$, and $\mu = 2.4 \times 10^{-4}$.

(or $\bar{E}_m$) are plotted with log$x$ scale in Figs. 6(*c*) and 6(*d*), respectively, with the other three variables fixed. In Fig. 6(*c*), it is evident that when $\mu > 0.008$, i.e., $\gamma > 138 \, \text{mJ/m}^2$, FC mode can be achieved but when $\mu < 0.0016$, i.e., $\gamma < 30 \, \text{mJ/m}^2$, the membrane would not conform to the substrate at all. Figure 6(*d*) indicates that when $\alpha < 0.2$, i.e., $\bar{E}_m < 10 \, \text{kPa}$, FC happens but when $\alpha > 2.5$, i.e., $\bar{E}_m > 125 \, \text{kPa}$, there is no conformability. It is also noted that the abrupt transition from FC to PC is also present in Figs. 6(*c*) and 6(*d*), with the same maximum contact area (23% of total surface area) under PC. In summary, Fig. 6 offers a quantitative guideline toward conformable skin-mounted electronics in the four-parameter design space.

3.2 PI Membrane on a Feline Brain In Vivo. In addition to human skin, brain is another soft organ with surface roughness that can prevent intracranial electrodes from conformal contact with the cortex. To retrieve electrocorticography with high spatial–temporal resolution, Kim et al. [10] fabricated ultrathin PI supported gold electrode arrays on a bioabsorbable film of silk fibroin. The silk substrate was gradually dissolved after being mounted on the cortex and hence left the ultrathin electrodes wrapping the cortex tissue due to the capillary adhesion. Since the gold layer is only 150 nm thick, which is much thinner than the thinnest PI they used (2.5 μm), the gold layer is neglected in the following conformability discussion. The conformability of electrodes with two different PI thicknesses (2.5 μm and 76 μm) was tested on a feline brain in vivo. It turned out that the 2.5 μm thickness electrodes achieved full conformability to the feline brain, while the 76 μm thick electrode was not able to conform at all. According to the experimental pictures [10], roughness of the brain gyrus is determined to be $h_0 = 0.24$ mm and $\lambda = 11.86$ mm, which yields $\beta = 0.13$. By neglecting the gold

layer, the modulus of the electrodes is given by PI modulus: $\bar{E}_m = 2.8$ GPa [10]. The modulus of the brain is found in literature as $\bar{E}_s = 50$ kPa [37]. Hence, the membrane–substrate modulus ratio is computed as $\alpha = 56,000$. As for the interface intrinsic work of adhesion, since the PI substrate is washed by saline solution in the experiment and placed on the wet brain surface, we simply assume that the work of adhesion is twice of the surface energy of water at room temperature: $\gamma = 144 \, \text{mJ/m}^2$ which yields $\mu = 0.00024$.

The conformability of electrodes with three different thicknesses (2.5 μm, 12 μm, and 76 μm) laminated on cortex can be predicted by our theory by substituting $\beta = 0.13$, $\alpha = 56,000$, $\mu = 0.00024$, and $\eta = 0.0002$, 0.001, and 0.006 into Eq. (25). The normalized total energy $\hat{U}$ versus $\hat{x}_c$ and ξ is plotted in Figs. 7(*a*)–7(*c*). When $\eta = 0.0002$ (i.e., $t = 2.5 \, \mu m$) (Fig. 7(*a*)), global minimal energy falls at $\hat{x}_c = 1$ and $\xi = 0.9$ as labeled by the red dot. It means the electrode is predicted to fully conform to the brain while the brain was slightly flattened by reducing the amplitude to $h_1 = 0.9h_0$.

When $\eta = 0.001$ (i.e., $t = 12 \, \mu m$) (Fig. 7(*b*)), the global minimal minimum locates at $\hat{x}_c = 0.12$ and $\xi = 0.86$, as highlighted by the red dot in the figure, which indicates a PC scenario. When $\eta = 0.006$ (i.e., $t = 76 \, \mu m$) (Fig. 7(*c*)), the minimal energy occurs at $\hat{x}_c = 0$ and $\xi = 1$, suggesting that the membrane is not able to conform to the cortex at all. To offer a holistic picture of the effect of electrode thickness on conformability, Fig. 7(*d*) plots $\hat{x}_c$ as a function of η as the top axis and t as the bottom axis when $\beta = 0.13, \alpha = 56,000$, and $\mu = 0.00024$ are fixed. We use three black dots to represent the three different thicknesses of electrodes. Again, our prediction of conformability agrees well with the experimental findings. Figure 7(*d*) also tells that full conformability can only be achieved when $\eta < 0.0042$, i.e., the thickness of PI should be smaller than 5 μm. The sharp transition from FC to PC

modes again suggests that there is an upper limit in the maximum contact area (23% of the total surface area) under the PC condition and hence FC mode is strongly preferred for effective measurements and treatments.

4 Discussion

4.1 Double-Checking Assumption (ii) Under FC Condition. Assumption (ii) dictates that the substrate surface deforms from one sinusoidal shape to another sinusoidal shape over the contact zone. This is inspired by the FC scenario in which the substrate surface undergoes a sinusoidal deformation over the entire wavelength when the membrane is fully attached on it, in which case the traction exerted on the substrate is also sinusoidal and the substrate energy can be readily calculated [27]. Here, we would like to double check whether the surface displacement and traction are both sinusoidal under FC mode and whether our substrate energy can recover the result given in Ref. [27]. By setting $x_c = \lambda/2$, the displacement of the substrate surface becomes

$$u(x) = (h_1 - h_0)\left(1 + \cos\frac{2\pi x}{\lambda}\right), \quad 0 \le x \le \lambda/2 \quad (26)$$

And, the corresponding traction is

$$P(x) = P_1(x) + P_2(x) = \pi\bar{E}_s \frac{h_1 - h_0}{\lambda}\cos\frac{2\pi x}{\lambda}, \quad 0 \le x \le \lambda/2 \quad (27)$$

where

$$\begin{cases} P_1(x) = -\pi\bar{E}_s \dfrac{h_0 - h_1}{\lambda}\left(1 + \cos\dfrac{2\pi x}{\lambda}\right), & 0 \le x \le \lambda/2 \quad (28)\\ P_2(x) = \pi\bar{E}_s \dfrac{h_0 - h_1}{\lambda} \end{cases}$$

Therefore, elastic energy in the substrate $U_{\text{substrate}}$ (per unit arc length) can be calculated through the work done by the traction

$$U_{\text{substrate}} = \frac{1}{2\lambda}\int_0^\lambda P(x)u(x)dx = \frac{1}{4}\ \pi\bar{E}_s \frac{(h_0 - h_1)^2}{\lambda} \quad (29)$$

which is exactly the same as that obtained by nonlinear analysis of wrinkles [25] and linear perturbation method [26]. This outcome proves that from energy point of view, our method is validated as it can successfully decay to the FC solution.

4.2 Displacement of Substrate Surface in the Noncontacting Zone $(x_c \le x \le \lambda/2)$. Displacement of substrate surface within contact zone $(0 \le x \le x_c)$ is assumed to be Eq. (16) and corresponding traction with adhesion taken into account is given by Eqs. (17)–(20), whereas the noncontacting zone $(x_c \le x \le \lambda/2)$ has traction free surface. Then, displacement over noncontacting zone can be written as $u(x) = u_1(x) + u_2(x)$ where the displacement of $u_1(x)$ induced by $P_1(x)$ is given as [33]

$$u_1(x) = (h_1 - h_0)$$
$$\times \left[1 + \cos\frac{2\pi x}{\lambda} + 2\left(\sin\frac{\pi x_c}{\lambda}\right)^2 G(x)\right], \quad x_c \le x \le \lambda/2 \quad (30)$$

where

$$G(x) = \zeta\sqrt{\zeta^2 - 1} - \ln[\zeta + \sqrt{\zeta^2 - 1}], \quad x_c \le x \le \lambda/2 \quad (31)$$

with $\zeta(x) = (\sin \pi x/\lambda)/(\sin(\pi x_c)/\lambda)$. Since $u_2(x)$ induced by $P_2(x)$ is given as [33]

$$u_2(x) = 2(h_0 - h_1)\left(\sin\frac{\pi x_c}{\lambda}\right)^2 \ln\left[\zeta + \sqrt{\zeta^2 - 1}\right], \quad x_c \le x \le \lambda/2 \quad (32)$$

As a result, the noncontacting substrate surface displacement can be analytically expressed.

4.3 Thin Membrane Versus Thick Slab. In our 2D plane strain theory, the membrane is modeled as a Bernoulli–Euler beam (for 2D case, von Karman plate theory should be applied) which undergoes bending and stretching when laminated onto a corrugated substrate. This assumption is valid as long as the thickness of the membrane is much smaller than the wavelength of the corrugated substrate, i.e., $\eta = t/\lambda \ll 1$. However, when the thickness of the film is comparable or even larger than the wavelength of the substrate, this assumption no longer holds, which is referred as a thick slab. When a thick but soft slab is laminated on a corrugated substrate, the lower surface of the slab will deform to fill the cavity between the substrate while the upper surface of the slab will stay almost flat. As a result, the slab needs to be modeled as an elastic body instead of a beam (or plate). Hence, the total energy given by Eq. (25) is no longer reliable when, for example, $\eta = 2$ (i.e., $t = 500 \mu m$) in Fig. 6. The contact problems of a thin elastic plate and an elastic body making contact with a randomly rough hard surface were studied by Persson and coworkers [24], in which the elastic energy needed to deform a large thin plate U_{plate} and to deform a semi-infinite elastic solid U_{solid} so that they make full contact with a substrate cavity of diameter λ and height h are given as

$$U_{\text{plate}} \sim Et^3\left(\frac{h}{\lambda}\right)^2 \quad (33)$$

$$U_{\text{solid}} \sim E\lambda^3\left(\frac{h}{\lambda}\right)^2 \quad (34)$$

respectively, where E is the Young's modulus of the plate or solid on the top. If $t \ll \lambda$, the elastic energy stored in plate is much smaller than the elastic energy stored in a thick solid. Therefore, the thin plate is elastically softer than a thick slab and hence easier to conform to the substrate.

5 Conclusions

Using the method of energy minimization, this paper develops an analytical model to determine the conformability of a thin elastic membrane placed on a soft substrate with a slightly wavy surface. Four dimensionless governing parameters have being identified. Although the effect of each parameter is monotonic, abrupt transition from FC to PC has been observed for all the parameters. Analytical predictions of the conformability of Ecoflex membrane on Ecoflex-based skin replica and PI membrane on an in vivo feline brain have found excellent agreement with the experimental observations of conformability. Furthermore, critical membrane thickness, membrane–substrate intrinsic work of adhesion, and membrane to substrate stiffness ratio are identified for full conformability. This model hence provides a viable method to predict the conformability and contact area between thin elastic membrane and soft substrate with slightly wavy surface. It also offers a guideline for the design of the electronic membrane as well as the bio-electronic interface to achieve high conformability.

References

[1] Na, S. R., Suk, J. W., Ruoff, R. S., Huang, R., and Liechti, K. M., 2014, "Ultra Long-Range Interactions Between Large Area Graphene and Silicon," ACS Nano, **8**(11), pp. 11234–11242.

[2] Hendriks, C., and Franklin, S., 2010, "Influence of Surface Roughness, Material and Climate Conditions on the Friction of Human Skin," Tribol. Lett., **37**(2), pp. 361–373.

[3] Koenig, S. P., Boddeti, N. G., Dunn, M. L., and Bunch, J. S., 2011, "Ultrastrong Adhesion of Graphene Membranes," Nat. Nanotechnol., **6**(9), pp. 543–546.

[4] Gao, W., and Huang, R., 2011, "Effect of Surface Roughness on Adhesion of Graphene Membranes," J. Phys. D: Appl. Phys., **44**(45), p. 452001.

[5] Persson, B., 2003, "On the Mechanism of Adhesion in Biological Systems," J. Chem. Phys., **118**(16), pp. 7614–7621.

[6] Persson, B., and Gorb, S., 2003, "The Effect of Surface Roughness on the Adhesion of Elastic Plates With Application to Biological Systems," J. Chem. Phys., **119**(21), pp. 11437–11444.

[7] Scharfenberg, S., Rocklin, D., Chialvo, C., Weaver, R. L., Goldbart, P. M., and Mason, N., 2011, "Probing the Mechanical Properties of Graphene Using a Corrugated Elastic Substrate," Appl. Phys. Lett., **98**(9), p. 091908.

[8] Kim, D.-H., Ghaffari, R., Lu, N., and Rogers, J. A., 2012, "Flexible and Stretchable Electronics for Biointegrated Devices," Annu. Rev. Biomed. Eng., **14**(1), pp. 113–128.

[9] Xu, L., Gutbrod, S. R., Bonifas, A. P., Su, Y., Sulkin, M. S., Lu, N., Chung, H. J., Jang, K. I., Liu, Z., Ying, M., Lu, C., Webb, R. C., Kim, J. S., Laughner, J. I., Cheng, H., Liu, Y., Ameen, A., Jeong, J. W., Kim, G. T., Huang, Y., Efimov, I. R., and Rogers, J. A., 2014, "3D Multifunctional Integumentary Membranes for Spatiotemporal Cardiac Measurements and Stimulation Across the Entire Epicardium," Nat. Commun., **5**, p. 3329.

[10] Kim, D.-H., Viventi, J., Amsden, J. J., Xiao, J., Vigeland, L., Kim, Y.-S., Blanco, J. A., Panilaitis, B., Frechette, E. S., Contreras, D., Kaplan, D. L., Omenetto, F. G., Huang, Y., Hwang, K.-C., Zakin, M. R., Litt, B., and Rogers, J. A., 2010, "Dissolvable Films of Silk Fibroin for Ultrathin Conformal Bio-Integrated Electronics," Nat. Mater., **9**(6), pp. 511–517.

[11] Yang, S., Chen, Y. C., Nicolini, L., Pasupathy, P., Sacks, J., Becky, S., Yang, R., Daniel, S., Chang, Y. F., Wang, P., Schnyer, D., Neikirk, D., and Lu, N., 2015, "Cut-and-Paste Manufacture of Multiparametric Epidermal Sensor Systems," Adv. Mater., **27**(41), pp. 6423–6430.

[12] Kim, D. H., Lu, N., Ma, R., Kim, Y. S., Kim, R. H., Wang, S., Wu, J., Won, S. M., Tao, H., Islam, A., Yu, K. J., Kim, T. I., Chowdhury, R., Ying, M., Xu, L., Li, M., Chung, H. J., Keum, H., McCormick, M., Liu, P., Zhang, Y. W., Omenetto, F. G., Huang, Y., Coleman, T., and Rogers, J. A., 2011, "Epidermal Electronics," Science, **333**(6044), pp. 838–843.

[13] Jeong, J.-W., Yeo, W.-H., Akhtar, A., Norton, J. J. S., Kwack, Y.-J., Li, S., Jung, S.-Y., Su, Y., Lee, W., Xia, J., Cheng, H., Huang, Y., Choi, W.-S., Bretl, T., and Rogers, J. A., 2013, "Materials and Optimized Designs for Human-Machine Interfaces Via Epidermal Electronics," Adv. Mater., **25**(47), pp. 6839–6846.

[14] Yeo, W. H., Kim, Y. S., Lee, J., Ameen, A., Shi, L., Li, M., Wang, S., Ma, R., Jin, S. H., and Kang, Z., 2013, "Multi-Functional Electronics: Multifunctional Epidermal Electronics Printed Directly Onto the Skin," Adv. Mater., **25**(20), p. 2778.

[15] Huang, X., Cheng, H., Chen, K., Zhang, Y., Zhang, Y., Liu, Y., Zhu, C., Ouyang, S.-C., Kong, G.-W., Yu, C., Huang, Y., and Rogers, J. A., 2013, "Epidermal Impedance Sensing Sheets for Precision Hydration Assessment and Spatial Mapping," IEEE Trans. Biomed. Eng., **60**(10), pp. 2848–2857.

[16] Webb, R. C., Bonifas, A. P., Behnaz, A., Zhang, Y. H., Yu, K. J., Cheng, H. Y., Shi, M. X., Bian, Z. G., Liu, Z. J., Kim, Y. S., Yeo, W. H., Park, J. S., Song, J. Z., Li, Y. H., Huang, Y. G., Gorbach, A. M., and Rogers, J. A., 2013, "Ultrathin Conformal Devices for Precise and Continuous Thermal Characterization of Human Skin," Nat. Mater., **12**(10), pp. 938–944.

[17] Choi, S., Park, J., Hyun, W., Kim, J., Kim, J., Lee, Y. B., Song, C., Hwang, H. J., Kim, J. H., Hyeon, T., and Kim, D. H., 2015, "Stretchable Heater Using Ligand-Exchanged Silver Nanowire Nanocomposite for Wearable Articular Thermotherapy," ACS Nano, **9**(6), pp. 6626–6633.

[18] Hong, S., Lee, H., Lee, J., Kwon, J., Han, S., Suh, Y. D., Cho, H., Shin, J., Yeo, J., and Ko, S. H., 2015, "Highly Stretchable and Transparent Metal Nanowire Heater for Wearable Electronics Applications," Adv. Mater., **27**(32), pp. 4744–4751.

[19] Bandodkar, A. J., Molinnus, D., Mirza, O., Guinovart, T., Windmiller, J. R., Valdes-Ramirez, G., Andrade, F. J., Schoning, M. J., and Wang, J., 2014, "Epidermal Tattoo Potentiometric Sodium Sensors With Wireless Signal Transduction for Continuous Non-Invasive Sweat Monitoring," Biosens. Bioelectron., **54**, pp. 603–609.

[20] Huang, X., Liu, Y. H., Chen, K. L., Shin, W. J., Lu, C. J., Kong, G. W., Patnaik, D., Lee, S. H., Cortes, J. F., and Rogers, J. A., 2014, "Stretchable, Wireless Sensors and Functional Substrates for Epidermal Characterization of Sweat," Small, **10**(15), pp. 3083–3090.

[21] Son, D., Lee, J., Qiao, S., Ghaffari, R., Kim, J., Lee, J. E., Song, C., Kim, S. J., Lee, D. J., Jun, S. W., Yang, S., Park, M., Shin, J., Do, K., Lee, M., Kang, K., Hwang, C. S., Lu, N. S., Hyeon, T., and Kim, D. H., 2014, "Multifunctional Wearable Devices for Diagnosis and Therapy of Movement Disorders," Nat. Nanotechnol., **9**(5), pp. 397–404.

[22] Wagner, T. J., and Vella, D., 2012, "The Sensitivity of Graphene 'Snap-Through' to Substrate Geometry," Appl. Phys. Lett., **100**(23), p. 233111.

[23] Qiao, S. T., Gratadour, J. B., Wang, L., and Lu, N. S., 2015, "Conformability of a Thin Elastic Membrane Laminated on a Rigid Substrate With Corrugated Surface," IEEE Trans. Compon., Packag., Manuf. Technol., **5**(9), pp. 1237–1243.

[24] Carbone, G., Mangialardi, L., and Persson, B., 2004, "Adhesion Between a Thin Elastic Plate and a Hard Randomly Rough Substrate," Phys. Rev. B, **70**(12), p. 125407.

[25] Huang, Z. Y., Hong, W., and Suo, Z., 2005, "Nonlinear Analyses of Wrinkles in a Film Bonded to a Compliant Substrate," J. Mech. Phys. Solids, **53**(9), pp. 2101–2118.

[26] Xiao, J., Carlson, A., Liu, Z. J., Huang, Y., and Rogers, J. A., 2010, "Analytical and Experimental Studies of the Mechanics of Deformation in a Solid With a Wavy Surface Profile," ASME J. Appl. Mech., **77**(1), p. 011003.

[27] Wang, S. D., Li, M., Wu, J., Kim, D. H., Lu, N. S., Su, Y. W., Kang, Z., Huang, Y. G., and Rogers, J. A., 2012, "Mechanics of Epidermal Electronics," ASME J. Appl. Mech., **79**(3), p. 031022.

[28] Cheng, H., and Wang, S., 2013, "Mechanics of Interfacial Delamination in Epidermal Electronics Systems," ASME J. Appl. Mech., **81**(4), p. 044501.

[29] Tchvialevaa, L., Zenga, H., Markhvidaa, I., McLeana, D. I., Luia, H., and Leea, T. K., 2010, "Skin Roughness Assessment," New Developments in Biomedical Engineering, D. Campolo ed., InTech, Vukovar, Croatia, pp. 341–358.

[30] Johnson, K. L., 1995, "The Adhesion of Two Elastic Bodies With Slightly Wavy Surfaces," Int. J. Solids Struct., **32**(3–4), pp. 423–430.

[31] Westergaard, H., 1939, "Bearing Pressures and Cracks," ASME J. Appl. Mech., **66**, pp. 49–53.

[32] Koiter, W., 1959, "An Infinite Row of Collinear Cracks in an Infinite Elastic Sheet," Arch. Appl. Mech., **28**(1), pp. 168–172.

[33] Zilberman, S., and Persson, B., 2002, "Adhesion Between Elastic Bodies With Rough Surfaces," Solid State Commun., **123**(3), pp. 173–177.

[34] Jeong, J. W., Kim, M. K., Cheng, H. Y., Yeo, W. H., Huang, X., Liu, Y. H., Zhang, Y. H., Huang, Y. G., and Rogers, J. A., 2014, "Capacitive Epidermal Electronics for Electrically Safe, Long-Term Electrophysiological Measurements," Adv. Healthcare Mater., **3**(5), pp. 642–648.

[35] Yu, Y. L., Sanchez, D., and Lu, N. S., 2015, "Work of Adhesion/Separation Between Soft Elastomers of Different Mixing Ratios," J. Mater. Res., **30**(18), pp. 2702–2712.

[36] Scharfenberg, S., Mansukhani, N., Chialvo, C., Weaver, R. L., and Mason, N., 2012, "Observation of a Snap-Through Instability in Graphene," Appl. Phys. Lett., **100**(2), p. 021910.

[37] Pailler-Mattei, C., Bec, S., and Zahouani, H., 2008, "In Vivo Measurements of the Elastic Mechanical Properties of Human Skin by Indentation Tests," Med. Eng. Phys., **30**(5), pp. 599–606.